sustainability

MDPI

Article

An Approach to a New Supplementary Cementing Material: *Arundo donax* Straw Ash

Jordi Payá [1,*], Josefa Roselló [2], José María Monzó [1], Alejandro Escalera [1], María Pilar Santamarina [2], María Victoria Borrachero [1] and Lourdes Soriano [1]

[1] Grupo de Investigación en Química de los Materiales (GIQUIMA), Instituto de Ciencia y Tecnología del Hormigón ICITECH, Universitat Politècnica de València, Valencia E-46022, Spain; jmmonzo@cst.upv.es (J.M.M.); alescru@gmail.com (A.E.); vborrachero@cst.upv.es (M.V.B.); lousomar@upvnet.upv.es (L.S.)

[2] Departamento de Ecosistemas Agroforestales, Universitat Politècnica de València, Valencia E-46022, Spain; jrosello@upvnet.upv.es (J.R.); mpsantam@eaf.upv.es (M.P.S.)

* Correspondence: jjpaya@cst.upv.es; Tel.: +34-963877564

Received: 27 September 2018; Accepted: 15 November 2018; Published: 19 November 2018



Abstract: *Arundo donax* is a plant native to Asia and is considered an invader species in the Mediterranean region and many tropical zones in the world. These invader plants can be collected to produce a biomass, which can be converted to ash by combustion. The scope of the study is to assess the use of these ashes (*Arundo donax* straw ash [ADSA]) as supplementary cementing material due to their relatively high silica content. Electron microscopy studies on dried and calcined samples of different plant parts (cane, sheath leaf and leaf) were carried out. Some different cellular structures were identified in the spodogram (remaining skeleton after calcination). Major silica content was found in leaves and sheath leaves. The main element in all the ashes studied, together with oxygen, was potassium (22 to 46% depending on the part of the plant). Chloride content was also high (5–13%), which limits their use to non-steel reinforced concrete. The pozzolanic reactivity of ADSA was assessed in pastes by thermogravimetric analysis and in mortars with ordinary Portland cement based on compressive strength development. Excellent results were found in terms of reactivity.

Keywords: biomass ash; pozzolan; spodogram

1. Introduction

It is well known that certain plants are considered invasive species and lead to many problems in ecosystems. In many cases, these plants were introduced into several regions several hundred years ago. Some examples in the Mediterranean region are *Opuntia* sp., *Agave* sp. and *Arundo donax*. The last example was introduced into Europe from South Asia and is naturally abundant in India, China, Iran and Turkey, among other countries. This species is a Liliopsidae class (also known as Monocotyledonae) and belongs to the order Poales, the family Poaceae and the subfamily Arundinoideae. It is commonly known as giant reed (also known as bamboo reed, giant cane, Spanish reed, wild cane). In Spanish, it is known as "caña común", "caña de Castilla" or "cañabrava". This plant had several uses in ancient times: basketry, making paper pulp, fencing gardens, fishing rods and as tutor supports for plants in tomato or bean orchards. In construction, the cane was also used in drop ceilings, sunshades and floors [1].

Nowadays, *Arundo donax* has expanded to the worldwide tropical zones of South Africa, South America and the United States (US) and also to the Caribbean and Pacific Islands [2]. It is also very common in the Mediterranean zone. In the last decade, there has been great interest in developments related to biofuel and biomass from this fast-growing plant [3,4]. Krička et al. [4]

reported that biomass from *Arundo donax* can be utilised as solid biofuel: it had a high lignin content (33.65%, this means that this biomass is more suitable for direct combustion), and appropriate coke and fixed carbon percentages (13.18% and 11.37%, respectively). Adversely, the remaining ash content was high (3.56%) which could diminish the quality of the resulting fuel.

Interestingly, *Arundo donax* absorbs considerable quantities of silica from the soil during its growth [5]. Consequently, it is an interesting source of reactive ashes for building materials (e.g., as a pozzolanic component in blended Portland cements or as a source of silica in geopolymeric systems). The combustion of *Arundo donax* straw (composed of cane, leaf sheaths and leaves) yields the corresponding ash (*Arundo donax* straw ash [ADSA]), which has interesting chemical and mineralogical compositions from a reactivity point of view.

There are many interesting examples of ashes produced from biomass combustion, some of which have pozzolanic properties due to their amorphous silica content [6]. The best known example is rice husk ash (RHA) [7]. Other ashes have been studied to assess their properties in terms of their reactivity in cementing systems. These include sugarcane bagasse ash (SCBA), studied in ordinary Portland cement (OPC) mixes [8,9], and sugarcane straw ash (SCSA), studied in geopolymeric systems based on blast furnace slag [10]. Rice straw ash (RSA) has been characterized and used to replace 10% and 25% OPC [11]. Wheat straw ash and corncob ash were studied by Memon et al. [12,13] and demonstrated good pozzolanic performance of the ash, aiding in the production of environmentally friendly concrete. Elephant grass ash (EGA) has been studied in terms of pozzolanic reactivity and the development of eco-friendly cements [14–16]. Cordeiro et al. [14] found that the compressive strength of cement mortars with 20% replacement of EGA was slightly lower than reference mortar after 3 days of curing. However the behaviour of reference mortar and mortar containing EGA were similar for longer curing times (7 and 28 days).

Ismail and Jaeel studied the reuse of ash from giant reed [17] for the partial replacement of sand in concrete (2.5–12.5% range by mass). The giant reed ash (GRA) was obtained by burning small pieces of air-dried giant reed at 700 °C using an electrical furnace. The ash particles were large and presented mean diameters of 1 mm. The presence of GRA drastically reduced the slump of fresh concrete because of the absorption and the non-uniform shape of these large ash particles. The dry density of concrete was also slightly reduced with increasing GRA content. The compressive and flexural strengths of concrete with GRA (2.5–7.5% replacement of sand), similar to or higher than the control values. The authors did not provide the chemical composition of GRA; however they affirmed that the organic matter was completely removed after burning. Probably, part of the organic matter produced a material similar to charcoal and this explains the size of the particles.

In this study, different plant parts from the *Arundo donax* species were studied after drying and combustion treatments. Samples of cane, sheath leaf and leaf were dried at 105 °C and were also fired at 450 °C (to remove organic compounds). Optical and field emission scanning electron microscopy (FESEM) and energy-dispersive X-ray (EDX) spectroscopy analyses were carried out and identified the distribution of silicon and other elements in cellular tissues and cellules. The accumulation of silicon dioxide (silica gel, [5]) in some specific cells or parts of cells was mainly studied (i.e., phytoliths). The presence of other elements, i.e., potassium, calcium and chlorine, was analysed. The reactivity of ashes was assessed by thermogravimetric analysis of calcium hydroxide/ADSA paste and OPC/ADSA paste and by examining compressive strength development in OPC mortars that contained ADSA, replacing 25% of OPC.

2. Materials and Methods

An *Arundo donax* plant (mature) was collected from Valencia, near to the Universitat Politècnica de València (Figure 1a). From this plant, selected samples of sheath leaf (Figure 1b), leaf (Figure 1b) and cane (Figure 1c,d) were taken. They were dried at 105 °C in a stove for 24 h: the moisture content was in the 20–35% range by mass. Parts of the dried material were calcined in a furnace at 450 °C for 1 h: the remaining ash was in the 6–8% range by mass. The samples listed in Table 1 were analysed using

microscopy techniques. For the FESEM, selected samples (dried materials and ashes) were studied using a ZEISS ULTRA 55 microscope. Samples (covered by carbon) were studied at 2 kV and at a working distance of 4–7 mm. Samples for chemical microanalysis (EDX) were studied at 15 kV.

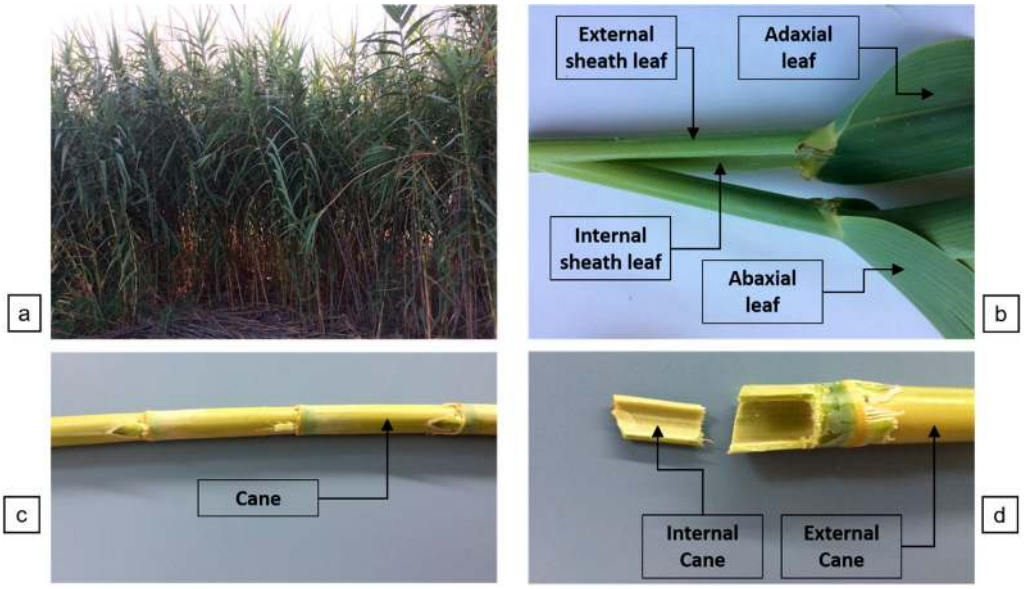


Figure 1. Images of the *Arundo donax* plant including selected parts used for the study: (**a**) group of plants; (**b**) parts of sheath leaf and leaf; (**c**) cane; (**d**) internal and external parts of cane.

Table 1. Samples of *Arundo donax* for analysis using microscopic techniques.

Treatment	Plant Part	Key	Observations
Dried at 105 °C	Cane	C-E C-I	External part Internal part
	Sheath leaf	S-E S-I	External part Internal part
	Leaf	L-Ab L-Ad	Abaxial part Adaxial part
Calcined at 450 °C	Cane	AC-E AC-I	Ash skeleton of the external part Ash skeleton of the internal part
	Sheath leaf	AS-E AS-I	Ash skeleton of the external part Ash skeleton of the internal part
	Leaf	AL-Ab AL-Ad	Ash skeleton of the abaxial part Ash skeleton of the adaxial part

An ADSA sample was obtained by calcination (autocombustion) of a large number of leaves and sheath leaves, which were separated from the cane. The plants were collected in the Turia river, close to the city of Paterna, 15 km from Valencia. The ash obtained was milled to reduce the mean particle diameter to 13.6 μm. The particle diameters for selected percentiles in volume of the ground ash were d(0.1) = 1.23 μm, d(0.5) = 7.50 μm and d(0.9) = 35.22 μm. This sample was chemically characterized. Pastes of ADSA with calcium hydroxide ($Ca(OH)_2$) and with OPC were prepared and characterized by thermogravimetry. Thermogravimetric analyses—thermogravimetric (TG) and differential thermogravimetric (DTG) curves—were carried out in an 850 TGA thermobalence (Mettler-Toledo, Zurich, Switzerland) using sealed pinholed aluminium crucibles. The heating range was 35–600 °C with a heating rate of 10 °C/min. OPC mortars were prepared and tested after 28 and 90 days of curing at 20 °C and 100% relative humidity (RH). Control mortars (only OPC, Spanish CEM I-52.5R) and mortar with 25% replacement ADSA were tested. Mortars (16 × 16 × 4 cm^3) in

which 25% of OPC was replaced by limestone filler were also prepared to assess dilution effects. Three specimens were tested for flexural strength and the six resulting parts were tested on compression for each curing age.

3. Results and Discussion

3.1. FESEM Analysis of Dried Samples at 105 °C

Selected samples of dried plant parts were studied by means of FESEM. Due to the morphology of these parts, micrographs were taken from the internal and external sides (see Table 1). Cane showed a corrugated external side (C-E, Figure 2a), with small holes and protuberances (Figure 2b). The internal side was flatter (C-I, Figure 2c), with small creases. Removing the epidermal tissue, an internal cellular distribution was observed (Figure 2d). In this internal distribution, there were some perforations in the cell wall (known as pits).

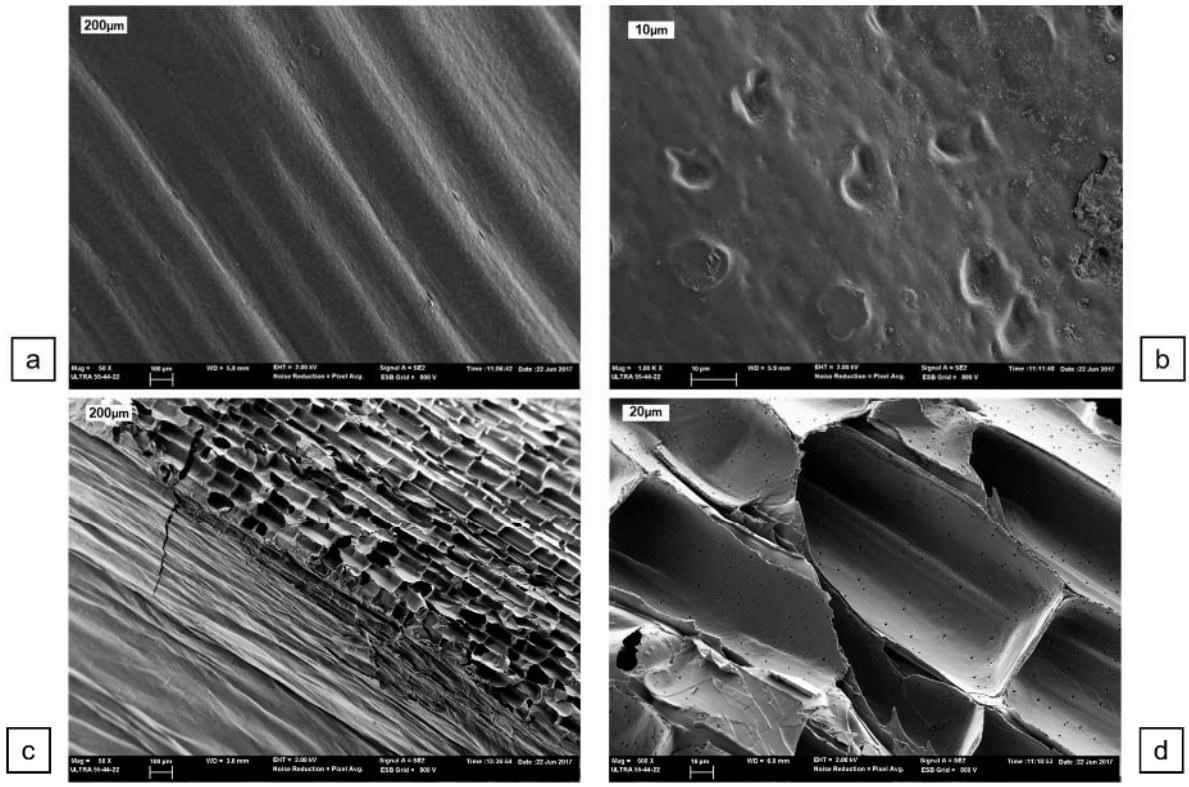


Figure 2. Field emission scanning electron microscopy (FESEM) micrographs of *Arundo donax* cane dried at 105 °C: (**a**) general view of the external part (C-E); (**b**) detailed view of C-E with holes and protuberances; (**c**) general view of the internal part (C-I) containing a zone with the intact epidermis and a zone without it showing the internal cellular structure; (**d**) detailed view of the internal cellular structure with perforations (pits).

The external part of the sheath leaf also presents (S-E, Figure 3a) a corrugated appearance similar to that found for C-E. The surface exhibited some special formations: elliptical elongated cells with undulated walls (cw) and some tetralobate (cross-shaped, p4) phytoliths (Figure 3b). The internal part of the sheath leaf (S-I, Figure 3c) presented a particular mapped structure showing the disposition of the epidermal cells. These cells presented undulated walls and a rectangular elongated shape (Figure 3d).

Finally, the abaxial side of the leaf (L-Ab, Figure 4a) also showed a corrugated disposition (similar to C-E and S-E), with aligned stomata (s) and some tetralobate phytoliths (p4) arranged between these

lines (Figure 4b). In the adaxial part of the leaf (L-Ad, Figure 4c), a similar alignment was found, with the presence of some hairs, i.e., long-thin trichomes (tl) (Figure 4d).

3.2. FESEM Analysis of Calcined Samples at 450 °C

Some dried plant parts were burned in an air atmosphere at 450 °C to remove the organic matter and leave the inorganic skeletons (spodograms). As before, both sides of the different plant parts were studied (see Table 1). Both ashes from cane (AC-E and AC-I, Figure 5) showed a similar skeleton, with the presence of rounded particles 5–10 μm in diameter. EDX analysis showed that these particles were very rich in potassium oxide (K_2O). Also these particles contained potassium chloride (KCl). EDX data from spots other than particles (dotted arrows in Figure 5) showed a high content of chlorine. No presence of silicon was determined in these analysis spots.

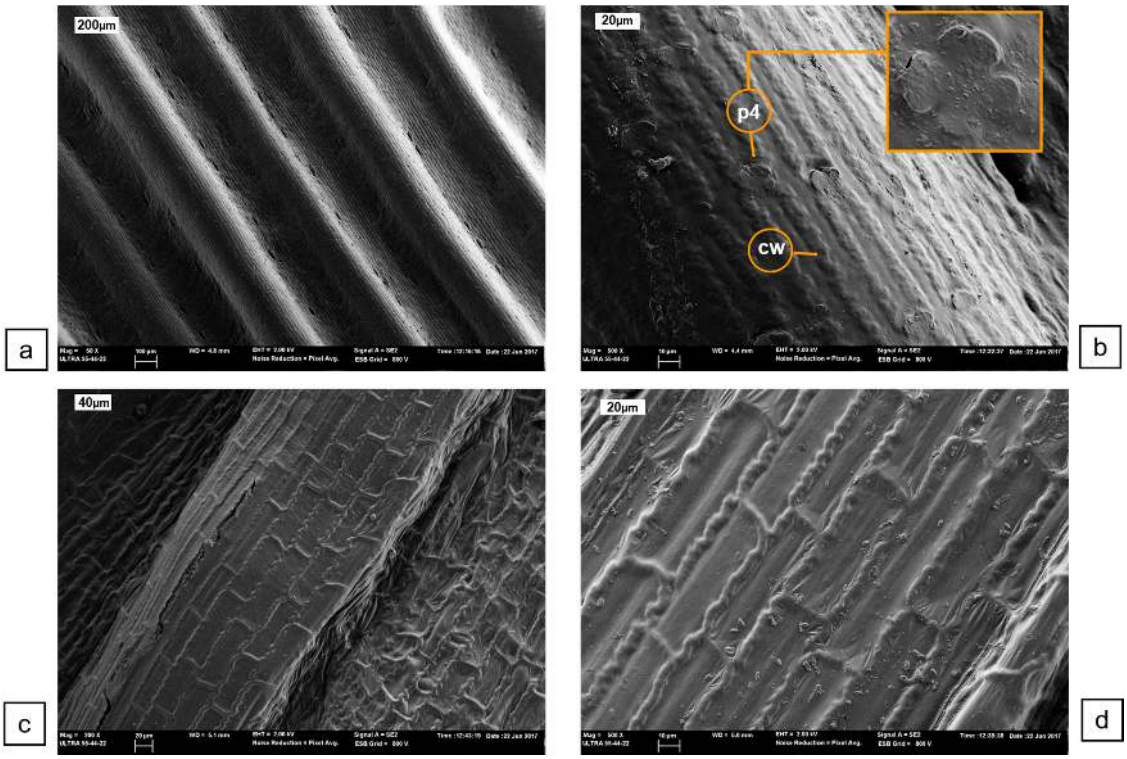


Figure 3. Field emission scanning electron microscopy (FESEM) micrographs of the *Arundo donax* sheath leaf dried at 105 °C: (**a**) general view of the external part (S-E) showing the corrugated structure; (**b**) detailed view of the S-E, showing tetralobate phytoliths (p4) and the undulated cell wall (cw); (**c**) general view of the internal part (S-I); (**d**) detailed view of the mapped structure, showing the elongated rectangular-shaped cells.

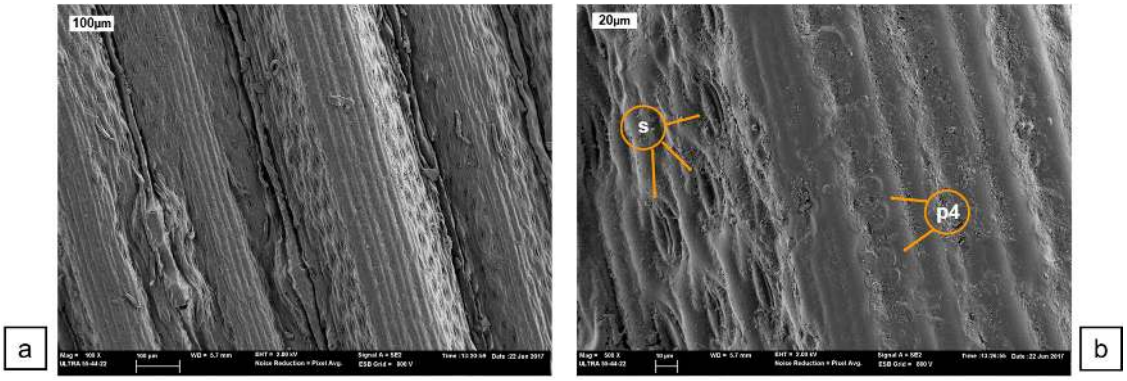


Figure 4. *Cont.*

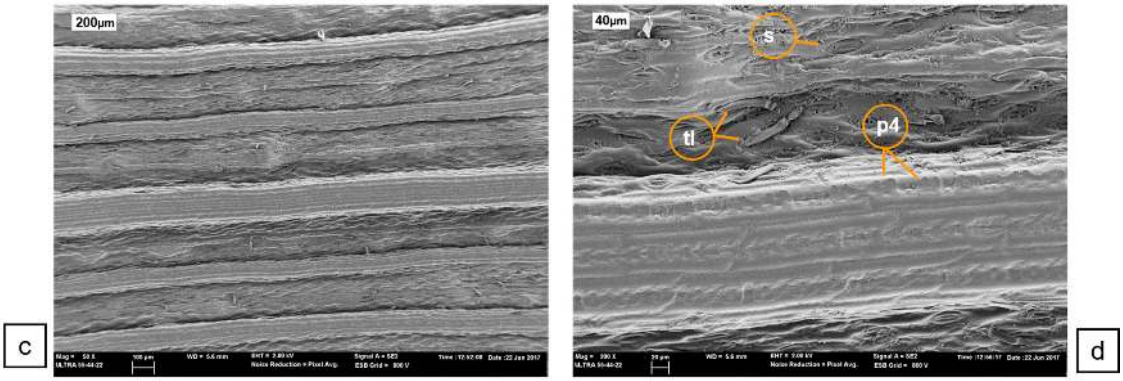


Figure 4. Field emission scanning electron microscopy (FESEM) micrographs of the *Arundo donax* leaf dried at 105 °C: (**a**) general view of the abaxial part (L-AB), (**b**) detailed view of L-Ab showing the stomata (s) and tetralobate phytoliths (p4); (**c**) general view of the adaxial part (L-Ad); (**d**) detailed view of L-Ad showing the presence of long-thin trichomes (tl).

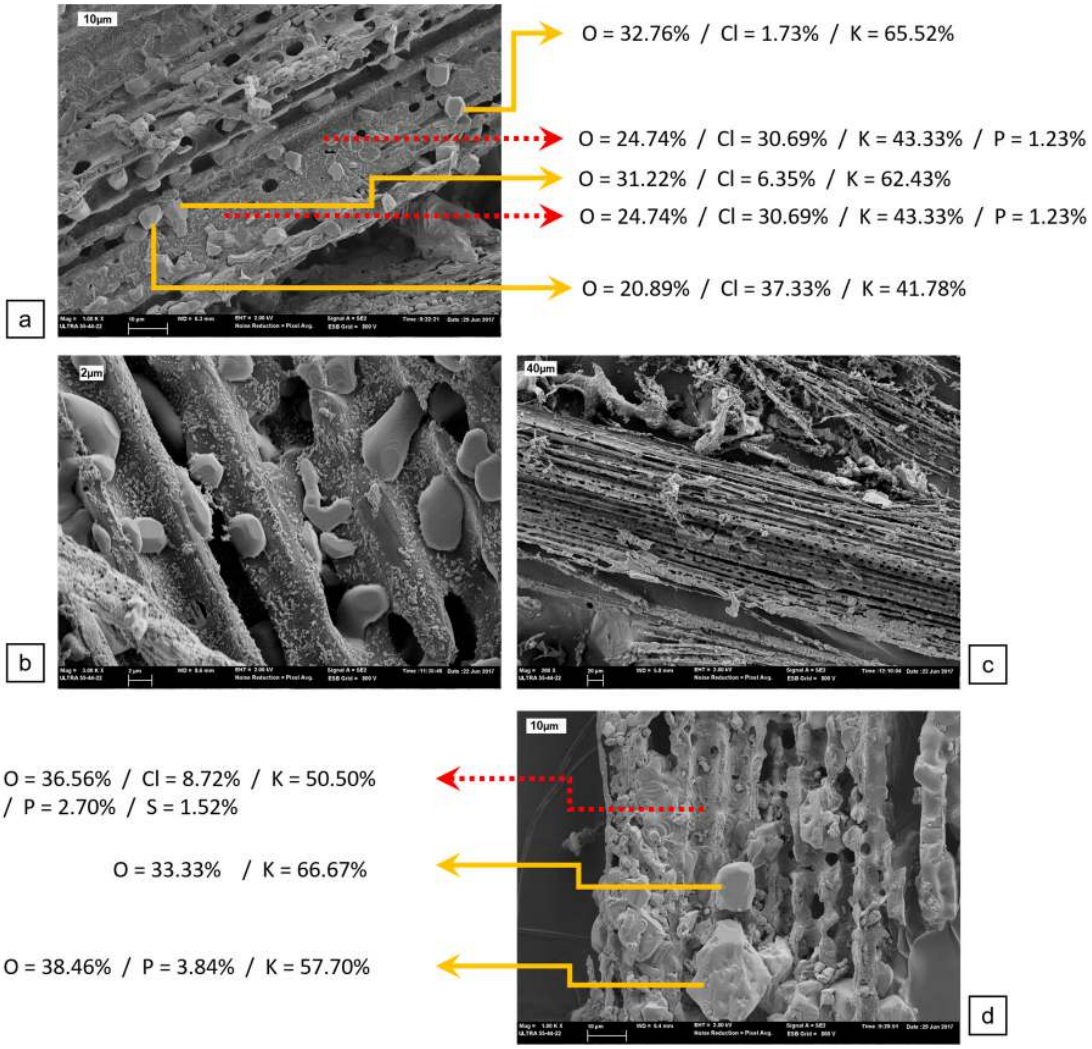


Figure 5. Field emission scanning electron microscopy (FESEM) micrographs of ash skeletons obtained from *Arundo donax* cane calcined at 450 °C: (**a**) general view of the external part (AC-E) with spot chemical compositions determined by energy dispersive X-ray (EDX); (**b**) detailed view of the particles; (**c**) general view of the internal part (AC-I); (**d**) detailed view of the particles with spot chemical compositions determined by EDX.

The external part of the sheath leaf (AS-E, Figure 6a,b) showed that many stomata remained after removing organic matter. These were rich in silicon and potassium (Figure 6a, EDX data). There were also many bilobate phytoliths, which presented the highest content of silicon (Figure 6a, EDX data, %Si = 30.93%). The magnification of one phytolith (Figure 6c) showed the presence of a layer in its surface rich in potassium. This tends to mean that the EDX data taken for the phytolith contain both silicon and potassium. The zones among stomata and phytoliths presented higher content of chlorine, potassium and some other elements, such as sulphur, phosphoros and magnesium (Figure 6a, EDX data, see dotted line). For the internal part of the sheath leaf, the surface layer of cells was removed from S-I (see Figure 3c,d). Many bilobate (p2) and tetralobate (p4) phytoliths appeared (AS-I, Figure 6d) under this layer after calcination. Figure 6e presented many phytoliths, analysed by EDX. These analyses (6 spots) revealed the following chemical composition for the phytoliths: O = 61.0 ± 0.9%, Si = 26 ± 2%, S = 1.9 ± 0.8%, Cl = 0.8 ± 0.4%, K = 11.1 ± 1.7%.

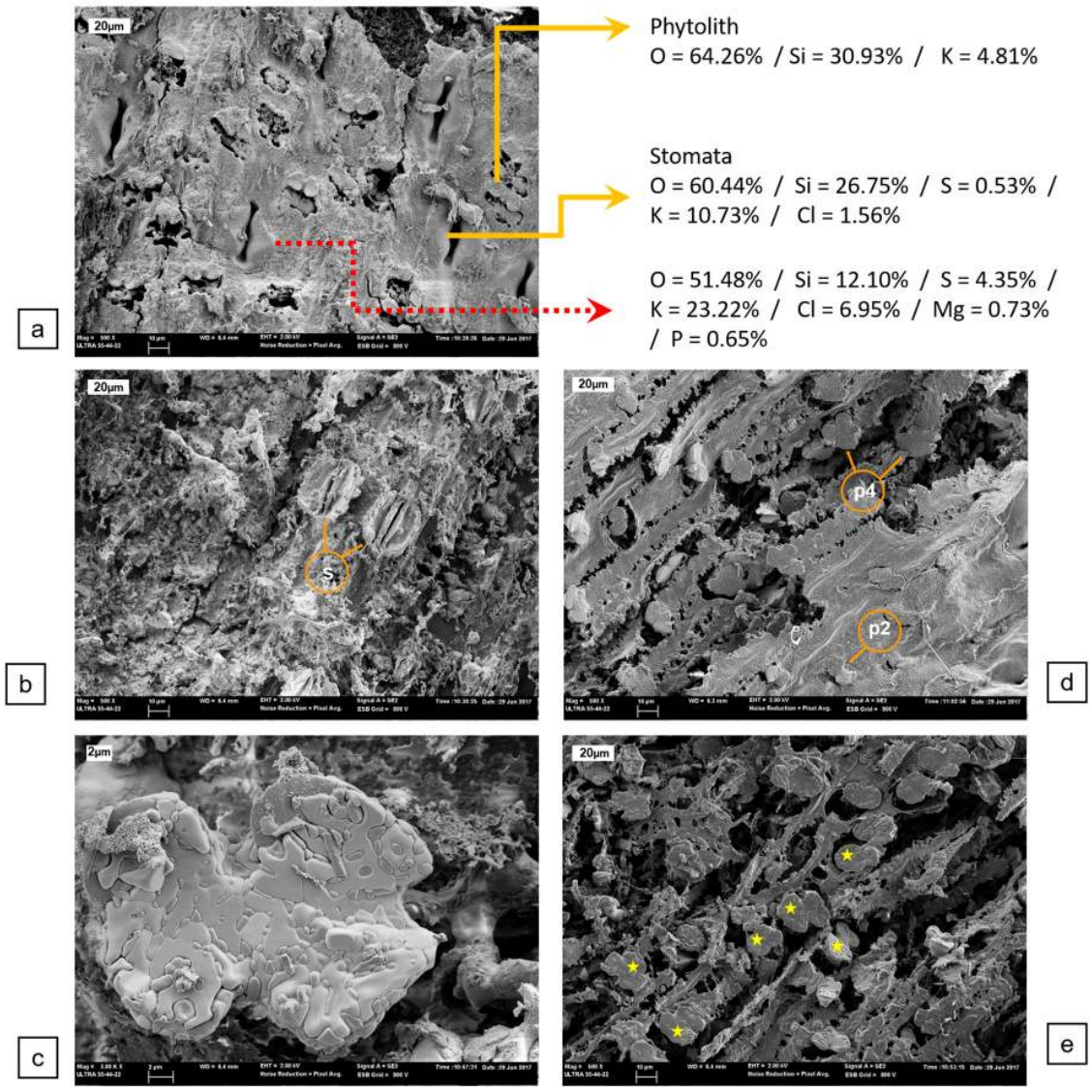


Figure 6. Field emission scanning electron microscopy (FESEM) micrographs of ash skeletons obtained from the *Arundo donax* sheath leaf calcined at 450 °C: (**a**) general view of the external part (AS-E) with spot chemical compositions determined by energy dispersive X-ray (EDX); (**b**) detailed view of the stomata (s); (**c**) detailed view of a phytolith; (**d**) general view of the internal part (AS-I) showing bilobate (p2) and tetralobate (p4) phytoliths; (**e**) spots on phytoliths (marked with stars).

Finally, abaxial and adaxial leaf ash samples (Figure 7) showed the presence of many aligned phytoliths. Many of these phytoliths were bilobated (Figure 7a,b) and they presented silicon as the main element (27–29%, see EDX spot data in Figure 7a), together with oxygen. These phytoliths were covered with particles rich in potassium and chloride. Some of the phytoliths (Figure 7c) were cross-shaped. They were distributed as chains and located in large nervadures. In the adaxial part (Figure 7d,e), there were also many phytoliths widely distributed in the spodogram. The zone surrounding the phytoliths was also rich in silicon (chemical composition spot from Figure 7a), with high potassium and chloride content and small amounts of sulphur and phosphorus.

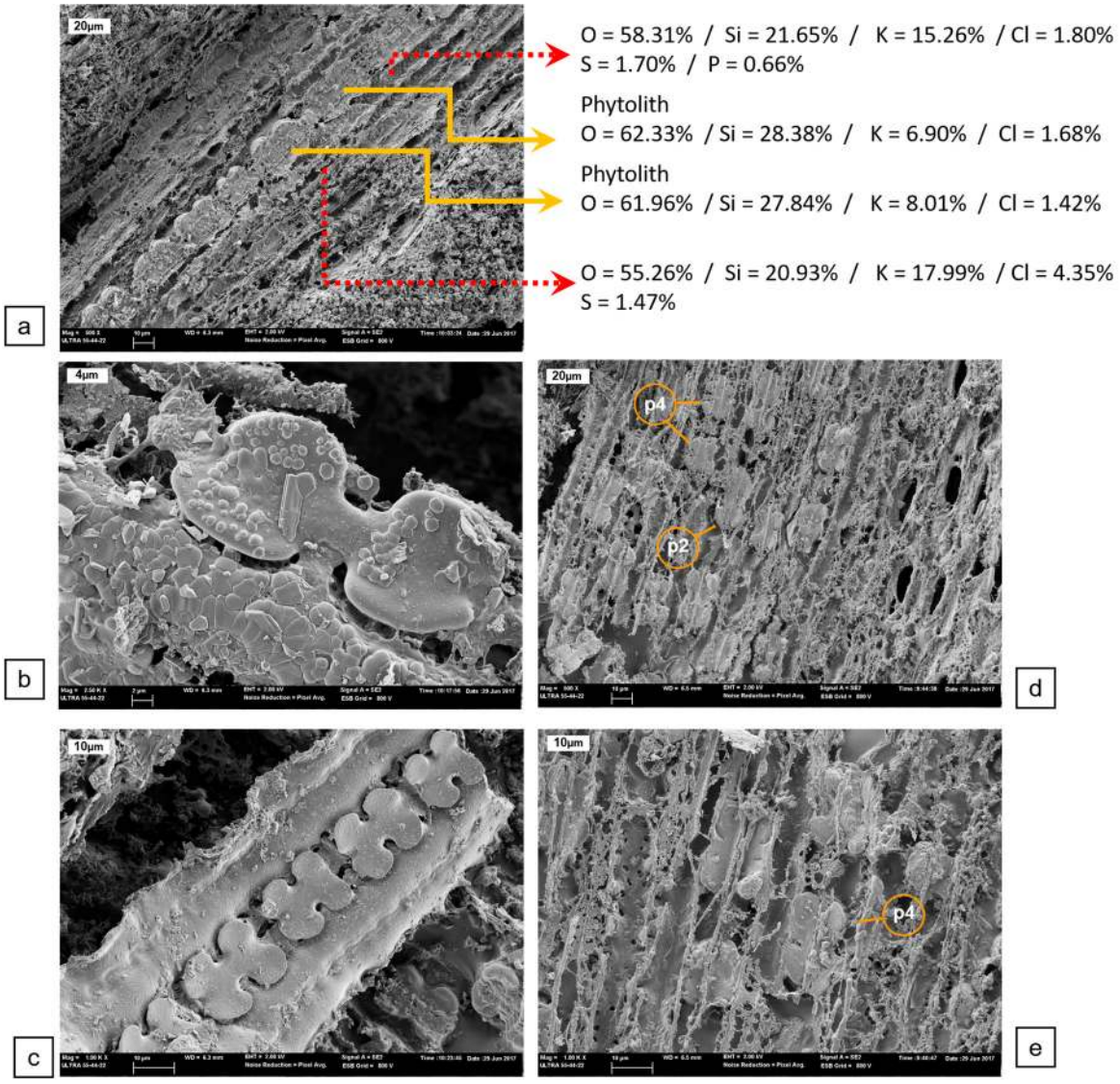


Figure 7. Field emission scanning electron microscopy (FESEM) micrographs of ash skeletons obtained from *Arundo donax* leaf calcined at 450 °C: (**a**) general view of the abaxial part (AL-Ab) with chemical composition energy spots determined by dispersive X-ray (EDX); (**b**) detailed view of a bilobate phytolith; (**c**) detailed view of a cross-shaped phytolith chain; (**d**) general view of the adaxial part (AL-Ad); (**e**) detailed view of phytoliths in the adaxial part. (Key: bilobate (p2) and tetralobate (p4) phytoliths).

Table 2 summarizes the chemical compositions of the samples determined by EDX. Analyses were calculated from data taken from an area of 10,000 µm^2 (mean value 10 data). In general, it can be observed that ashes are formed of oxygen, magnesium, silicon, phosphorus, sulphur, chlorine and

potassium, with sodium, aluminium and calcium not being significant elements in the composition. Aside from oxygen, potassium was the major element appearing in all ash samples, with composition ranges of 22–46%. This means that these ashes had an alkaline behaviour. The presence of high percentage of alkalis would enhance the dissolution rate of amorphous silica in ADSA, however in the case of the possibility of alkali-aggregate reaction (presence of reactive aggregates) a potential expansion must be taken into account. The chlorine content was also very high (5–13%). This means that the ashes from *Arundo donax* straw may not be used for reinforced concrete because of the critical danger of metallic corrosion.

In terms of silica content, ashes from cane (AC-E and AC-I) had very low values: less than 1%. This suggests that it is not useful to collect the cane together with other parts of the plant to produce ashes with relevant pozzolanic properties. Ashes from cane have high potassium chloride and potassium oxide content and they would be better used as raw materials for producing potassium-based fertilizer. Ashes from sheath leaves showed a different composition depending on the side studied: apparently, more silica is accumulated in the internal part (AS-I). With respect to the leaf, silica also appeared at a higher content level (15.39%) in the adaxial part of the leaf (AL-Ad); however the content on the other side (AL-Ab) was also high (9.76%). Both the AS and AL samples contained significant percentages of chlorine, which limits their use as supplementary cementing material for reinforced concrete.

The Cl/K atomic ratio for all studied samples was in the range 0.24–0.36 and the Si/K atomic ratio was higher than 0.40 for AS-I, AL-Ab and AL-Ad. This suggests that sheath leaves and leaves are the most interesting parts of the plant in terms of its use as a reactive component in cements. Interestingly, these ashes also have the lowest chloride content.

Ash classification by means of the Vassilev ternary diagram [18] is shown in Figure 8. In this diagram, the ashes from different parts of *Arundo donax* are located in the K zone, which corresponds to low-acid biomass ashes rich in potassium and chlorine. These ashes derived from *Arundo donax* are very different from those found for rice husk, sugar cane leaf and bamboo leaf [11].

Table 2. Energy dispersive X-ray (EDX) chemical analysis in atomic percentages and selected atomic ratios in different *Arundo* donax ash samples (mean and standard deviation [SD]).

Part	**AC-E**	**AC-I**	**AS-E**	**AS-I**	**AL-Ab**	**AL-Ad**
Element	**Mean (SD) ***	**Mean (SD) ***	**Mean (SD) ***	**Mean (SD) ***	**Mean (SD) ***	**Mean (SD) ***
O	37.42 (±1.06)	37.17 (±1.15)	47.15 (±2.25)	49.1 (±5.36)	51.06 (±4.28)	52.26 (±1.93)
Na	0 (0)	0 (0)	0.19 (±0.13)	0.03 (±0.08)	0 (0)	0 (0)
Mg	0 (0)	0.04 (±0.14)	1.55 (±0.58)	0.66 (±0.47)	1.34 (±0.61)	1.08 (±0.44)
Al	0 (0)	0 (0)	0.02 (±0.06)	0.01 (±0.05)	0.01 (±0.05)	0 (0)
Si	0.69 (±1.04)	0.11 (±0.23)	6.68 (±1.9)	11.03 (±7.64)	9.76 (±7.19)	15.39 (±3.63)
P	3.83 (±0.28)	4.2 (±1.07)	0.64 (±0.16)	0.43 (±0.27)	1.48 (±0.65)	1.25 (±0.54)
S	1.14 (±0.27)	1.43 (±0.64)	5.34 (±0.4)	4.19 (±1.93)	4.36 (±1.67)	2.01 (±0.94)
Cl	11.06 (±2.4)	12.83 (±2.4)	9.89 (±2.32)	8.91 (±3.69)	6.54 (±2.93)	5.52 (±1.54)
K	45.76 (±2.92)	44.19 (±2.49)	27.81 (±2.06)	25.58 (±6.88)	23.83 (±5.22)	22.47 (±3.2)
Ca	0 (0)	0 (0)	0.68 (±0.89)	0 (0)	1.57 (±0.73)	0 (0)
Atomic ratios						
Cl/K	0.24	0.29	0.36	0.35	0.27	0.25
Si/K	0.02	0.00	0.24	0.43	0.41	0.68

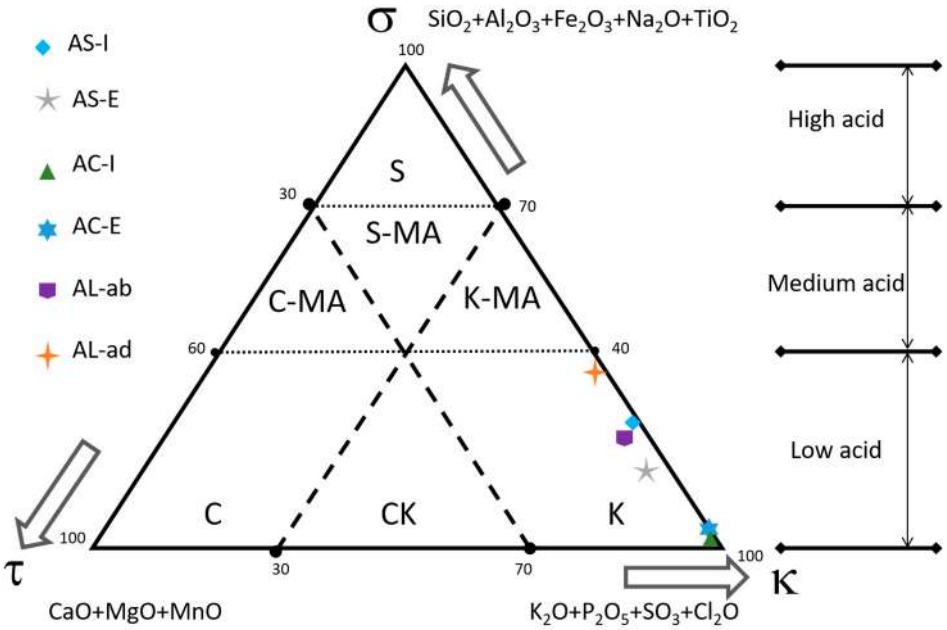


Figure 8. Ternary diagram for the classification of biomass ashes (according to [18]) indicating *Arundo donax*-derived ashes.

3.3. Pozzolanic Reactivity

A mixture of *Arundo donax* plant leaves and sheath leaves was used to prepare a large amount of ashes by autocombustion (Figure 9). After the combustion, the resulting material was sieved to remove the largest unburned particles. The mean particle diameter was 46.17 μm, a value usually too coarse for achieving pozzolanic reactivity. Then the ash was milled for 20 min in an alumina ball mill, yielding ADSA with a mean particle diameter of 13.57 μm. The loss on ignition of the ADSA was 11.4%. Figure 10 shows some micrographs from ashes before grinding. The shape and morphology of ashes are similar to those described for ashes obtained in furnace at 450 °C, even though many of the structures are broken, probably due to the higher temperature reached in the autocombustion container. The temperature reached during the autocombustion process was in the range 650-875ºC. Some particles showed evidence of sintering (Figure 10a). Bilobate phytoliths maintained their characteristic shape perfectly (Figure 10b,c). Some cellular walls with the typical undulated shape (Figure 10d) were also observed.



Figure 9. Autocombustion container: (**a**) *Arundo donax* leaves and sheath leaves before ignition; (**b**) remaining ashes after autocombustion.

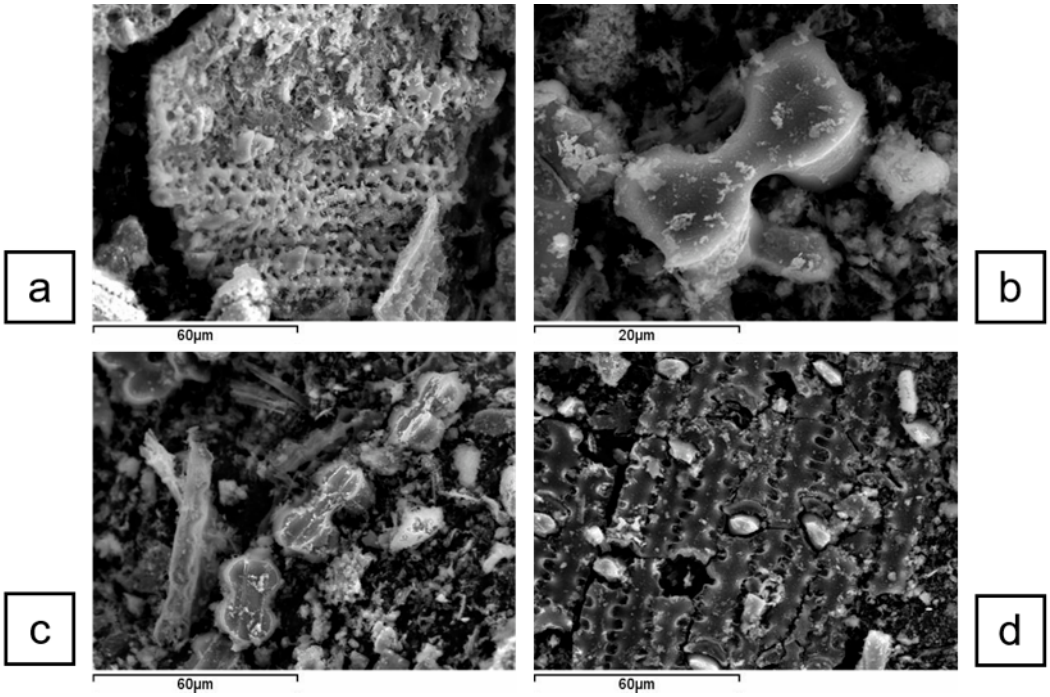


Figure 10. Particle morphologies found in autocombustion ashes before grinding: (**a**) sintered particle; (**b**) isolated bilobate phytolith; (**c**) bilobate phytoliths and irregular particles; (**d**) spodogram with undulated wall cells.

The chemical compositions were significantly different (Table 3), e.g., SiO_2 content was similar at 35.47% for ADSA and 24.78% for the value calculated from EDX data. The same was found for K_2O (29.54% vs. 44.70%). These differences are due to the plants growing in different soils. In addition, the CaO content for ADSA after autocombustion was much higher, due to soil nature and dust contamination (main calcium carbonate particles) in leaves and sheath leaves. In contrast, SO_3 was higher for samples taken close to Valencia, because the plants grew in a soil rich in gypsum and they took in sulphate ions through the roots.

Table 3. Chemical composition (by mass) of *Arundo donax* straw ash (ADSA) obtained by autocombustion (X-ray fluorescence [XRF] data) and the chemical composition of ashes obtained by means of a furnace at 450 °C (these values were calculated from EDX data in Table 2 as the average of AS-E, AS-I, AL-Ab and AL-Ad).

	XRF Data	EDX Data		XRF Data	EDX Data
Element	**%**	**%**	**Oxide**	**%**	**%**
Na	0.01	0.12	Na_2O	0.01	0.07
Mg	5.62	2.32	MgO	6.04	1.77
Al	0.34	0.03	Al_2O_3	0.41	0.03
Si	25.66	21.40	SiO_2	35.47	24.78
P	2.90	1.90	P_2O_5	4.29	2.62
S	1.27	7.94	SO_3	2.05	12.07
Cl	13.08	15.41	Cl_2O	10.34	12.76
K	37.99	49.75	K_2O	29.54	44.70
Ca	12.85	1.13	CaO	11.61	1.21
Fe	0.27	0.00	Fe_2O_3	0.25	0.00

Powder XRD pattern of ADSA obtained by autocombustion is shown in Figure 11. Several inorganic compounds were identified: silvite (KCl, pdfcard#411476) and arcanite (K_2SO_4, pdfcard#050613) as majoritary compounds and magnesite ($MgCO_3$, pdfcard#080479) and

hydroxylapatite ($Ca_5(PO_4)_3(OH)$, pdfcard#090432). Any crystalline silica (SiO_2) based compound was identified: this means that besides the temperature reached in the autocombustion process, silica did not crystallize (cristobalite, trydimite and any crystalline silicate were found). A baseline deviation in the 2θ range 23–35° was observed which suggests that silica was in the amorphous state.

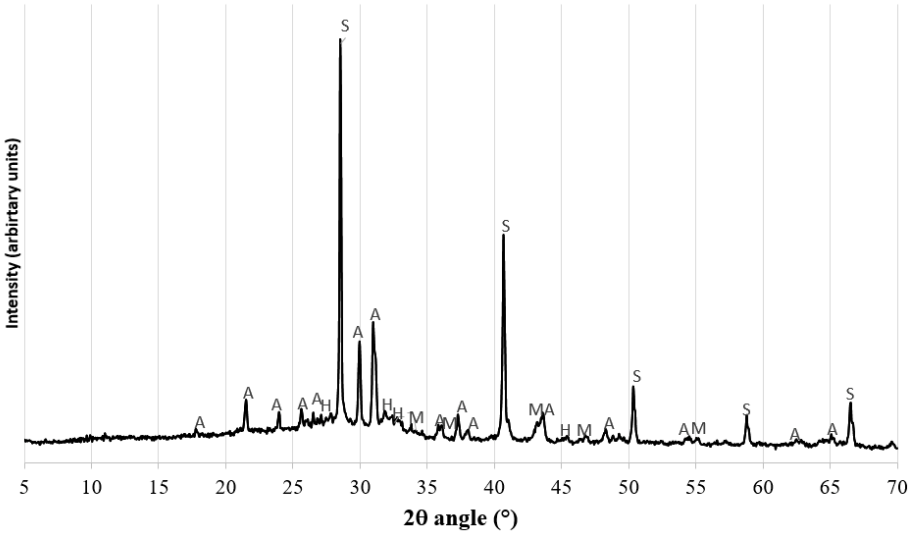


Figure 11. XRD pattern for ADSA. (Key: S: silvite; A: arcanite; M: magnesite; H: hydroxylapatite).

A paste with calcium hydroxide, $Ca(OH)_2$, was prepared containing an ADSA/$(Ca(OH)_2$ ratio of 1:2 and a water/binder ratio of 0.8. The paste was cured for 7 days at 40 °C. The TG and DTG curves are depicted in Figure 12. The total mass loss was 19.92%. The presence of water removed by heating, in the range 100–200 °C demonstrated that pozzolanic reaction products were formed due to the reaction between $Ca(OH)_2$ and the silica contained in ADSA. The mass loss (6.84%) observed in the range 530–590 °C was due to the dehydroxylation of the non-reactant $Ca(OH)_2$. From this value, the lime fixation can be calculated: the fixed lime was 57.9%. This result points to the high reactivity of ADSA in terms of pozzolanic behaviour. Similar results were found when the pozzolanic behaviour of sugarcane bagasse ash (SCBA) was analysed [19]: in this case with similar conditions, the fixed lime was in the range 42–45%.

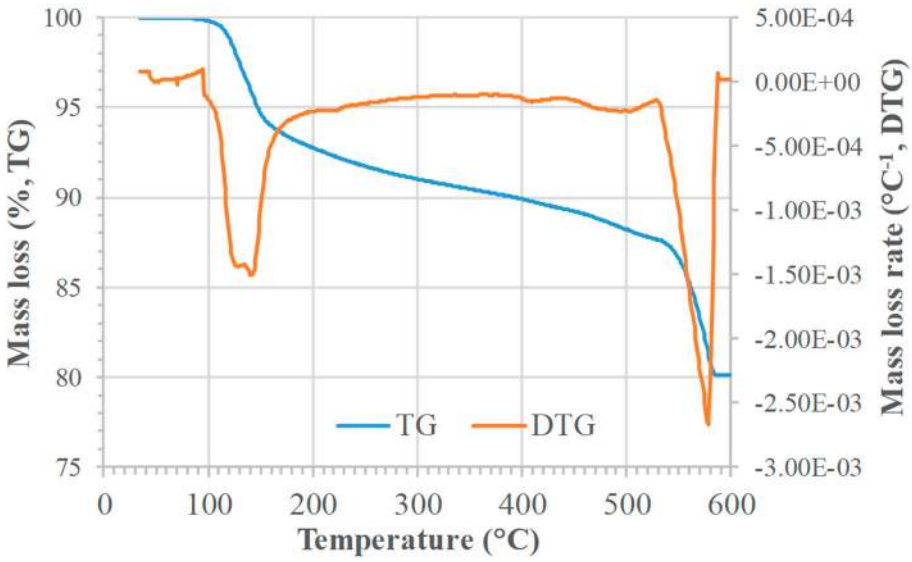


Figure 12. Thermogravimetric (TG) and differential thermogravimetric (DTG) curves for 1:2 *Arundo donax* straw ash/$Ca(OH)_2$ paste cured at 40 °C for 7 days.

The pozzolanic reactivity of ADSA in OPC paste was also analysed. A control paste, prepared with OPC with a water/binder ratio of 0.5 and cured for 7 days at 40 °C, presented the TG and DTG curves depicted in Figure 13. A total mass loss of 22.23% was obtained. A paste in which 30% of OPC was replaced by ADSA was also analysed. In this case, the total mass loss was 19.08% (see Figure 14). The mass loss related to $Ca(OH)_2$ dehydroxylation allowed the calculation of lime fixation, which was 38.9%. This demonstrated that the pozzolanic behaviour was also important, being higher than that typically obtained for pulverized coal fly ashes: Antiohos et al. [20] found lower fixed lime value for low calcium fly ash/OPC paste (20% replacement): about 25% after 90 days of curing.

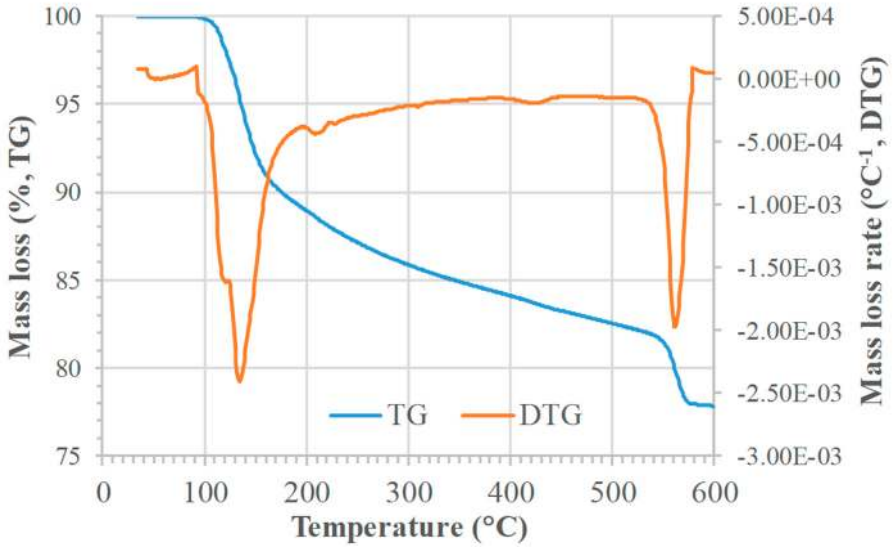


Figure 13. Thermogravimetric (TG) and differential thermogravimetric (DTG) curves for ordinary Portland cement (OPC) control paste cured at 40 °C for 7 days.

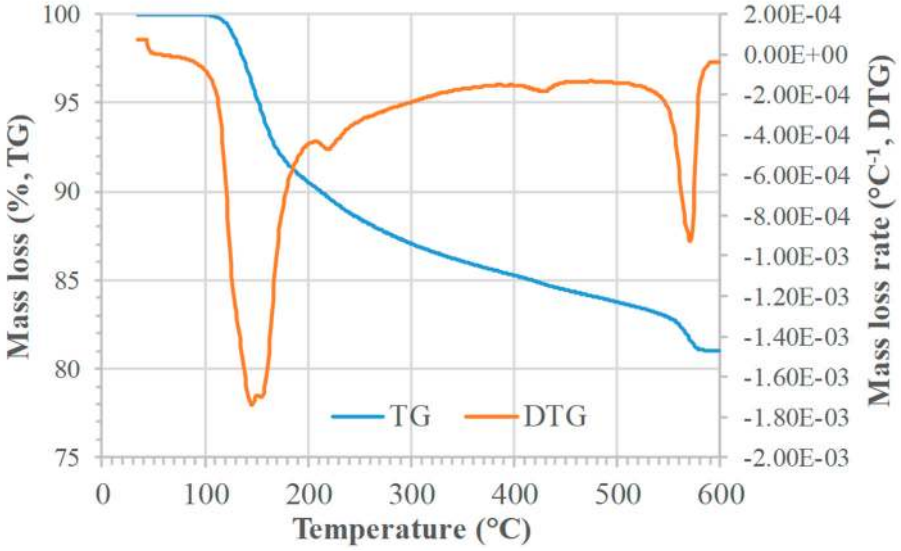


Figure 14. Thermogravimetric (TG) and differential thermogravimetric (DTG) curves for 30% *Arundo donax* straw ash (ADSA) replacement in ordinary Portland cement (OPC) paste cured at 40 °C for 7 days.

Finally, two mortars were prepared by mixing standardized sand (CEN EN UNE 196-1): one control mortar with OPC and the other in which 25% (by mass) of OPC was replaced with ADSA, both prepared with a water/binder ratio of 0.5. The water demand observed in the mortars with ADSA required the use of 1% of superplasticizer (GLENIUM ACE 31, by BASF). To assess the

effect on the mechanical properties of the sample with the replacement of OPC by ADSA, an additional mortar was prepared, replacing 25% (by mass) of OPC with limestone filler. These mortars were cured for 28 and 90 days at 20 °C in a 100% RH environment. The flexural and compressive strengths are summarized in Table 4.

Mortar containing ADSA yielded excellent strengths after both 28 and 90 days of curing. After 28 days, the ADSA containing mortar yielded better compressive strength (60.2 MPa) than the control sample (56.1 MPa), which highlights the reactivity of ADSA in cement-based binder. This trend was also maintained after 90 days of curing (65 vs. 59 MPa). The 28-day strength activity index [21,22] was 1.07, the typical value found for densified silica fume [23]. The 90-days strength activity index was 1.10. These strength values were similar than those found [8] for sugarcane straw ash (SiO_2 and LOI contents were 36.5% and 15.5% respectively, very similar to those found for ADSA).

The reactivity, in terms of strength development, of ADSA in OPC mixes was similar or higher to that observed for pulverized coal fly ash. Antiohos et al. [20] found that for fly ash mortars with 20% replacement, the compressive strength at 28 and 90 curing days was similar to the control, however, for a higher replacement rate (30%) the strength was lower (about 10%). Tangpagasit et al. [24], for mortars containing 20% of fly ash, found that for an original fly ash (median particle size of 19 μm) the strength activity index values after 28 and 90 days of curing were 0.81 and 0.91, respectively. These values were enhanced with the fineness of the fly ash by grinding (median particle size of 2.7 μm): 1.08 and 1.17 after 28 and 90 days of curing, respectively. Finally, De Weerdt et al. [25] studied the influence on compressive strength of standard mortars, replacing 5 to 35% of OPC by fly ash. They found that for percentages equal or lower than 15%, their strength was similar to control mortar (0% replacement), however for higher replacing percentages the strength decreased. The behaviour reported for different fly ashes [20,24,25] showed that the reactivity of ADSA was similar or higher than that observed for pulverized coal fly ashes.

Comparing the strength values of ADSA and filler mortars, one can note the high contribution of the ash to strength development. At 28 days of curing, the increase in strength was more than 20 MPa (a 50.9% increase) and at 90 days it was similar (46.4%). This means that the pozzolanic reaction was produced especially in the first 28 days of curing, denoting the high reactivity of ADSA. Despite the relatively low percentage of silica in ADSA, the mechanical contribution of the pozzolanic reaction was very high.

Table 4. Flexural and compressive strengths of mortars (control with only ordinary Portland cement (OPC); 25% replacement with *Arundo donax* straw ash (ADSA); 25% replacement with limestone filler) obtained after 28 and 90 days of curing at 20 °C in 100% relative humidity (RH).

Mortar	Flexural Strength (MPa)		Compressive Strength (MPa)	
	28 days	90 days	28 days	90 days
Control	6.8 ± 0.5	7.7 ± 0.5	56.1 ± 1.6	59 ± 2
25% ADSA	5.1 ± 0.5	7.0 ± 0.5	60.2 ± 1.2	65 ± 2
25% filler	6.1 ± 0.2	6.4 ± 0.2	40 ± 2	44.0 ± 1.4

4. Conclusions

Several parts of the *Arundo donax* plant (cane, sheath leaf and leaf) were analysed. FESEM studies on dried samples (105 °C) showed differences in the external morphology of both sides of each part. After calcination (450 °C) in controlled conditions, the resulting spodogram of the different parts was studied using FESEM. Different cells and cellular tissues were identified after calcination, suggesting that the resulting ashes had important content in the inorganic phase. Ashes from cane had the lowest content in terms of silicon, with potassium and chlorine being the main elements besides oxygen. Many particles of KCl and K_2O were identified by means of EDX. The internal part of the sheath leaf and the adaxial part of the leaf showed the highest content of silicon: many bilobate phytoliths were identified, which are mainly composed of SiO_2. Pozzolanic reactivity studies (thermogravimetry

and compressive strength development) showed excellent results. *Arundo donax* straw ash (ADSA) has interesting pozzolanic properties; however it contains high chloride content, which seriously limits its use in cements and concrete. It is thus only recommended for the preparation of non-steel reinforced concrete. In general, sheath leaves and leaves from *Arundo donax* are the most interesting parts for preparing reactive ashes and restrictions in terms of non-steel reinforced concrete must be taken into account.

Author Contributions: Conceptualization, J.P., J.R. and M.V.B.; methodology, J.M.M., L.S. and M.P.S.; formal analysis, J.P. and J.R.; investigation, J.M.M., A.E., L.S., M.V.B., J.R.; resources, M.V.B.; writing—original draft preparation, J.P. and J.R.; writing—review and editing, J.M.M., M.P.S., M.V.B. and L.S.; supervision, J.P.; project administration, M.V.B.

Funding: This research received no external funding.

Acknowledgments: The authors would like to thank the Electron Microscopy Service of the Universitat Politècnica de València.

Conflicts of Interest: The authors declare no conflict of interest.

References

1. González Bejarano, S.; Silva Delgado, E. *Arundo donax* L.: Material de construcción. Proyecto Final de Grado. Universitat Politècnica de Catalunya, Barcelona, Spain. 2012. Available online: https://core.ac.uk/download/pdf/41807621.pdf (accessed on 27 September 2018). (In Spanish)
2. Sanz Elorza, M.; Dana Sánchez, E.D.; Sobrino Vesperinas, E. *Atlas de las Plantas Alóctonas Invasoras en España*; Ministerio de Medio Ambiente, Dirección General para la Biodiversidad: Madrid, Spain, 2004; 384p, ISBN 84-8014-575-7. (In Spanish)
3. Angelini, L.G.; Ceccarini, L.; Bonari, E. Biomass yield and energy balance of giant reed (*Arundo donax* L.) cropped in central Italy as related to different management practices. *Eur. J. Agron.* **2005**, *22*, 375–389. [CrossRef]
4. Krička, T.; Matin, A.; Bilandžija, N.; Jurišić, V.; Antonović, A.; Voća, N.; Grubor, M. Biomass valorisation of *Arundo donax* L., Miscanthus × giganteus and Sida hermaphrodita for biofuel production. *Int. Agrophys.* **2017**, *31*, 575–581. [CrossRef]
5. Chauhan, D.K.; Tripathi, D.K.; Kumar, D.; Kumar, Y. Diversity, distribution and frequency based attributes of phytolith in *Arundo donax* L. *Int. J. Innov. Biol. Chem. Sci.* **2011**, *1*, 22–27.
6. Payá, J.; Monzó, J.; Borrachero, M.V. Outstanding aspects on the use of rice husk ash and similar agrowastes in the preparation of binders. In Proceedings of the Pro-Africa Conference: Non Conventional Building Materials Based on Agroindustrial Wastes, Pirassununga, Brazil, 18–19 October 2010.
7. Zain, M.F.M.; Islam, M.N.; Mahmud, F.; Jamil, M. Production of rice husk ash for use in concrete as a supplementary cementitious material. *Constr. Build. Mater.* **2011**, *25*, 798–805. [CrossRef]
8. Moraes, J.C.B.; Akasaki, J.L.; Melges, J.L.P.; Monzó, J.; Borrachero, M.V.; Soriano, L.; Payá, J.; Tashima, M.M. Assessment of sugar cane straw ash (SCSA) as pozzolanic material in blended Portland cement: Microstructural characterization of pastes and mechanical strength of mortars. *Constr. Build. Mater.* **2015**, *95*, 670–677. [CrossRef]
9. Cordeiro, G.C.; Toledo Filho, R.D.; Tavares, L.M.; Fairbaim, E.M.R. Pozzolanic activity and filler effect of sugar cane bagasse ash in Portland cement and lime mortars. *Cem. Concr. Compos.* **2008**, *30*, 410–418. [CrossRef]
10. Pereira, A.; Akasaki, J.L.; Melges, J.L.P.; Tashima, M.M.; Soriano, L.; Borrachero, M.V.; Monzó, J.; Payá, J. Mechanical and durability properties of alkali-activated mortar based on sugarcane bagasse ash and blast furnace slag. *Ceram. Int.* **2015**, *41*, 13012–13024. [CrossRef]
11. Roselló, J.; Soriano, L.; Santamarina, M.P.; Akasaki, J.L.; Monzó, J.; Payá, J. Rice straw ash: A potential pozzolanic supplementary material for cementing systems. *Ind. Crops Prod.* **2017**, *103*, 39–50. [CrossRef]
12. Memon, S.A.; Wahid, I.; Khan, M.K.; Tanoli, M.A.; Bimaganbetova, M. Environmentally friendly utilization of wheat straw ash in cement-based composites. *Sustainability* **2018**, *10*, 1322. [CrossRef]
13. Memon, S.A.; Khan, M.K. Ash blended cement composites: Eco-friendly and sustainable option for utilization of corncob ash. *J. Clean. Prod.* **2018**, *175*, 442–455. [CrossRef]

14. Cordeiro, G.C.; Sales, C.P. Pozzolanic activity of elephant grass ash and its influence on the mechanical properties of concrete. *Cem. Concr. Compos.* **2015**, *55*, 331–336. [CrossRef]
15. Cordeiro, G.; Sales, C.P. Influence of calcining temperature on the pozzolanic characteristics of elephant grass ash. *Cem. Concr. Compos.* **2016**, *73*, 98–104. [CrossRef]
16. Nakanishi, E.Y.; Frías, M.; Santos, S.F.; Rodrigues, M.S.; Villa, R.V.V.; Rodriguez, O.; Savastano, H., Jr. Investigating the possible usage of elephant grass ash to manufacture the eco-friendly binary cements. *J. Clean. Prod.* **2016**, *116*, 236–243. [CrossRef]
17. Ismail, Z.Z.; Jaeel, A.J. A novel use of undesirable wild giant reed biomass to replace aggregate in concrete. *Constr. Build. Mater.* **2014**, *67 Part A*, 68–73. [CrossRef]
18. Vassilev, S.V.; Baxter, D.; Andersen, L.K.; Vassileva, C.G. An overview of the chemical composition of biomass. *Fuel* **2010**, *89*, 913–933. [CrossRef]
19. Payá, J.; Monzó, J.; Borrachero, M.; Díaz-Pinzón, L.; Ordóñez, L. Sugar-cane bagasse ash (SCBA): Studies on its properties for reusing in concrete production. *J. Chem. Technol. Biotechnol.* **2002**, *77*, 321–325. [CrossRef]
20. Antiohos, S.; Maganari, K.; Tsimas, S. Evaluation of blends of high and low calcium fly ashes for use as supplementary cementing materials. *Cem. Concr. Compos.* **2005**, *27*, 349–356. [CrossRef]
21. AENOR. *Fly Ash for Concrete. Part 1: Definition, Specifications and Conformity Criteria*; UNE-EN 450-1; AENOR: Madrid, Spain, 2013.
22. AENOR. *Silica Fume in Concrete. Part 1: Definitions, Requirement and Conformity Criteria*; UNE-EN 13263-1; AENOR: Madrid, Spain, 2009.
23. Zhang, Z.; Zhang, B.; Yan, P. Comparative study of effect of raw and densified silica fume in the paste, mortar and concrete. *Constr. Build. Mater.* **2016**, *105*, 82–93. [CrossRef]
24. Tangpagasit, J.; Cheerarot, R.; Jaturapitakkul, C.; Kiattikomol, K. Packing effect and pozzolanic reaction of fly ash in mortar. *Cem. Concr. Res.* **2005**, *35*, 1145–1151. [CrossRef]
25. De Weerdt, K.; Kjellsen, K.O.; Sellevold, E.; Justnes, H. Synergy between fly ash and limestone powder in ternary cements. *Cem. Concr. Compos.* **2011**, *33*, 30–38. [CrossRef]



© 2018 by the authors. Licensee MDPI, Basel, Switzerland. This article is an open access article distributed under the terms and conditions of the Creative Commons Attribution (CC BY) license (http://creativecommons.org/licenses/by/4.0/).